

# Guiding Medical Needles Using Single-Point Tissue Manipulation

Meysam Torabi<sup>1</sup>, Kris Hauser<sup>2</sup>, Ron Alterovitz<sup>3</sup>, Vincent Duindam<sup>2</sup>, and Ken Goldberg<sup>4</sup>

**Abstract**—This paper addresses the use of robotic tissue manipulation in medical needle insertion procedures to improve targeting accuracy and to help avoid damaging sensitive tissues. To control these multiple, potentially competing objectives, we present a phased controller that operates one manipulator at a time using closed-loop imaging feedback. We present an automated procedure planning technique that uses tissue geometry to select the needle insertion location, manipulation locations, and controller parameters. The planner uses a stochastic optimization of a cost function that includes tissue stress and robustness to disturbances. We demonstrate the system on 2D tissues simulated with a mass-spring model, including a simulation of a prostate brachytherapy procedure. It can reduce targeting errors from more than 2cm to less than 1mm, and can also shift obstacles by over 1cm to clear them away from the needle path.

## I. INTRODUCTION

Needle insertion is a widely-used minimally invasive medical procedure with applications in tissue sample removal and therapy delivery. Its success depends largely on the physician’s skill and (often) luck. Procedures that require precise needle-tip positioning can fail due to improper positioning of the needle insertion point or by needle deflection as it travels through tissue. Furthermore, the target may shift due to tissue deformation from friction along the needle shaft, the patient’s breathing, or the patient’s involuntary movements. Procedures can be difficult even under imaging guidance. Breast and abdominal biopsies fail to sample malignancies in approximately 10% of insertions [8], [12]. Furthermore, straight-line needle paths may pass through sensitive tissues, such as arteries, nerves, or certain organs, to reach the target. Damaging these tissues may cause undesirable side effects.

In this paper, we investigate the use of robot-controlled tissue manipulation during needle insertion procedures. Tissue manipulators may be used to shift the target’s location in the tissue to improve *accuracy*. They could also be used to improve target *accessibility* by pushing obstacles and sensitive tissues away from the needle path. Tissue manipulation can be used alongside other promising techniques, such as model-based optimization of needle insertion parameters [3],

This work is supported in part by the National Institute of Health under NIH grant R01 EB006435 and NIH grant F32 CA124138, and by the Netherlands Organization for Scientific Research

<sup>1</sup> School of Electrical Engineering, Sharif University of Technology, Tehran, Iran. mtorabi@alum.sharif.edu

<sup>2</sup> Department of Electrical Engineering and Computer Science, University of California at Berkeley. {hauser@berkeley.edu, v.duindam@ieee.org}

<sup>3</sup> Department of Computer Science, University of North Carolina at Chapel Hill. ron@cs.unc.edu

<sup>4</sup> Department of Electrical Engineering and Computer Science and the Department of Industrial Engineering and Operations Research, University of California at Berkeley. goldberg@berkeley.edu

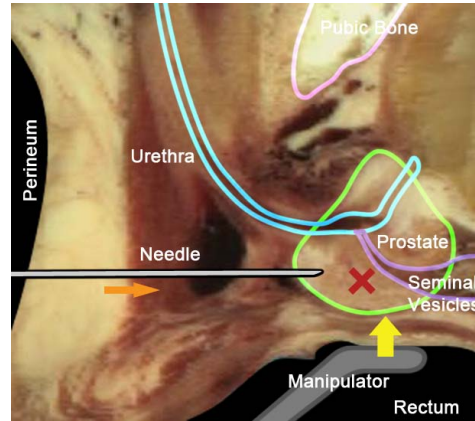


Fig. 1. Sagittal slice of a needle insertion procedure with tissue manipulation in a prostate cancer brachytherapy application. A cross depicts the seed’s target location. Image from The Visible Human Project.

applying external forces on the shafts of flexible needles [7], [9], and steering flexible bevel-tip needles [15], [17]. Specifically, we consider image-guided, straight line, rigid-needle insertions using one or more manipulators.

Our primary motivation is an application to prostate cancer brachytherapy (see Fig. 1). In low dose rate (LDR) brachytherapy, dozens of needle insertions are used to insert radioactive seeds into the prostate. Seed locations are carefully preplanned to deliver a sufficient radioactive dose to cancerous regions, and minimize the dose absorbed by surrounding tissues. With manual insertions under ultrasound guidance, the average seed placement error is approximately 0.63cm [16], which is about 15% of the width of the prostate. This placement error may cause excess radiation to be absorbed by the urethra and reproductive organs, contributing to the risks of incontinence and sexual dysfunction. We consider using a single manipulator within the rectum (depicted in gray in Fig. 1) to help guide the needle insertion in order to reduce targeting errors. Furthermore, the manipulator may also be used to guide the needle around sensitive structures within the prostate, which could further diminish side effects.

We consider a single-manipulator, closed-loop controller that uses 2D imaging feedback (typically ultrasound, fluoroscopy, or magnetic resonance imaging) to position a single point in the tissue. Even though only one point is moved at a time, the system uses a phased operation that sequentially pushes sensitive tissues away from the needle path, and finally corrects for residual needle targeting errors. The method could be applied to prostate and other cancer treatments as well as biopsies of the breast [13] or abdominal organs. We analyze several design choices in terms of their clinical applicability, such as whether compression,

shearing, or tension manipulation forces are preferable. Our technical contributions include an approximation of the set of attainable displacements of points in the tissue. This approximation is valid for small, quasistatic deformations and linearly elastic tissues. We also present a preoperative procedure planner that optimizes the placement of the needle and manipulators, given a geometric and physical model of the tissue and manipulator.

We evaluate our controller in simulation using 2D mass-spring models, including a simulation of a prostate brachytherapy procedure. These experiments suggest that single-point tissue manipulation can reduce targeting error to the order of one millimeter and helps the needle avoid sensitive tissue while reaching relatively inaccessible targets.

## II. RELATED WORK

Several researchers are studying methods for improving needle insertion accuracy using robotics technology. Most similar to our work, Mallapragada et. al. applied tissue manipulation to improve targeting accuracy for a breast biopsy procedure [13]. Their technique was based on the control of multiple frictionless contact points; we use a similar feedback control strategy, but consider moving only one manipulator at a time, in phases. We also consider manipulation via friction and/or tension forces, and manipulation of obstacles to improve accessibility. Thus, the scope of our work addresses a broader range of clinical procedures, which requires additional preoperative planning.

In preoperative planning, Alterovitz et. al. chooses the needle insertion location and depth to compensate for tissue deformation, using a 2D tissue simulation and numerical optimization [3]. Dehghan and Salcudean optimized needle insertion pose using a 3D tissue simulation [6]. DiMaio and Salcudean and Glozman and Shoham investigated the use of external forces on the needle shaft to guide a flexible needle [7], [9]. External tissue manipulation could be used in conjunction with both these techniques. Preoperative optimizations depend largely on the accuracy of tissue simulation; tissue manipulation can correct for modeling errors during the procedure. Tissue and needle manipulations may be used together to reduce stress on both needle and tissue.

Steerable needles are another approach to improving accessibility as well as targeting accuracy [1], [15], [17]. Bevel-tip flexible needles can be steered inside soft tissue by controlling insertion angle and velocity. Like tissue manipulation, these techniques have the potential to improve accuracy and to avoid complex obstacles. However, they require thin needles to be used, are hard to control, and may not follow predictable curved paths in all tissue types.

## III. OVERVIEW

We consider a procedure where a rigid needle is inserted into soft tissue to reach a target inside the body. The needle may be controlled by a physician or a robotic device. An imaging device provides real-time visual feedback. A manipulator system applies forces to the tissue to help guide the needle.

We consider a control system that moves a single manipulator at a time. It proceeds in phases, where in each phase, the controller attempts to move the position of one point in the tissue (called a *point of interest*) onto the needle path. In the initial phases, sensitive tissues are moved away from the needle path as the needle is inserted. The final phase corrects for targeting errors, by using the target location as the point of interest. In each phase, the controller uses a tissue model to determine feedforward forces at the manipulator, and uses PI feedback to correct for modeling errors and deformations.

The controller can address a wide range of clinical procedures, as long as care is taken to select a proper needle insertion path and each phase's manipulation device(s), manipulation points, and points of interest. We choose these parameters using an automated procedure planner that uses a numerical optimization to improve robustness and reduce tissue stress. It uses a model-based reachability analysis that, for a given manipulator, approximately determines the set of attainable displacements of targets in the tissue.

## IV. SINGLE-PHASE MANIPULATOR CONTROL

The single-phase controller operates a single manipulator  $M$  to drive a single *point of interest*  $p$  in the tissue directly toward the needle path. We use the method of Hirai and Wada [11], which computes a feedforward manipulator displacement based on a deformable model of the tissue. We combine this method with an integral term that drives the steady state error toward zero.

### A. Assumptions

The controller assumes that the manipulator uses translation without rotation to directly command the position of one or more points  $c_1, \dots, c_k$  in the tissue. This means that if the manipulator uses unilateral contact (pushing), the contact must not slip or break. This must be ensured by preoperative planning, as described in Sec. V.

The needle location and the point of interest are assumed to be measured accurately. Needles show up clearly in imaging, so standard computer vision techniques suffice. Estimating the locations of points in the tissue, however, require the use of deformable image registration techniques [2].

We assume that deformation can be essentially considered quasistatic, so the tissue's internal forces are in equilibrium with the applied manipulation force. This is justified when the needle and manipulator move at low velocity and the deformation is highly damped. We assume the manipulator moves precisely along a prescribed trajectory.

### B. Linearized Quasistatic Feedforward Model

This section describes the method of Hirai and Wada [11], with a small extension to handle points that do not lie directly on simulation nodes. The method computes a feedforward manipulator displacement that achieves a desired target displacement, assuming a linearized, quasistatic mass-spring model of the tissue. Specifically, let  $q$  be a generalized coordinate representation of the deformable object's state (e.g,  $q$  parameterizes a finite element or a mass-spring model).

We will show that a displacement  $\delta m$  of the manipulator position is related to the resulting displacement  $\delta p$  of the point of interest by a linear equation  $\delta p = A(q)\delta m$ .

The equations of quasistatic equilibrium are  $\sum_{i=1}^k J_i^T(q)f_i + g(q) = 0$ , where  $f_i$  is the force applied on the tissue at point  $c_i$ ,  $J_i$  is the Jacobian of  $c_i$  with respect to  $q$ , and  $g(q)$  is the vector of internal forces determined by some constitutive model. For mass-spring models and finite element models with linear elements, all  $J_i$  are constant, so we drop the dependence on  $q$ . For convenience, we rewrite the formula as

$$J^T f + g(q) = 0 \quad (1)$$

where we have stacked the  $f_i$ 's into a column vector  $f$  and stacked the  $J_i$ 's in a larger matrix  $J$ .

Consider a fixed state  $q$ , and let  $f^0$  denote the equilibrium forces currently applied at the manipulation points. In other words,  $f^0$  solves for  $f$  in (1). Consider trying to achieve an infinitesimal displacement  $\delta p$  of  $p$  by shifting  $M$  by an infinitesimal displacement  $\delta m$ . The change in the deformable object's state  $\delta q$  can be determined as follows. After the shift, the equilibrium force  $f^1$  at the manipulator solves the equation  $J^T f^1 + g(q + \delta q) = 0$ . Substituting  $g(q) = -J^T f^0$  in a first order Taylor expansion of  $g(q)$ , we have

$$J^T(f^1 - f^0) + dg/dq(q)\delta q = 0.$$

The Jacobian  $dg/dq(q)$  is the negation of the *stiffness matrix*  $-K(q)$ , and is symmetric positive definite. By inversion,

$$\delta q = K(q)^{-1}J^T(f^1 - f^0) \quad (2)$$

Let  $J_p$  be the Jacobian of  $p$  with respect to  $q$ . Substituting (2) in the definition  $\delta p = J_p\delta q$ , we get

$$\delta p = J_p K(q)^{-1}J^T(f^1 - f^0) \quad (3)$$

Now, assume all of  $c_1, \dots, c_k$  move by the manipulator's shift  $\delta m$ . That is,  $\delta m = J_i\delta q$  for  $i = 1, \dots, k$ . Let  $B_k$  be the  $kd \times d$  matrix of  $k$  stacked identity matrices of size  $d$  ( $d=2$  or  $3$ , depending on the world's dimension). Then:

$$B\delta m = J\delta q = JK(q)^{-1}J^T(f^1 - f^0)$$

Solving for  $f^1 - f^0$  and substituting the result in (3), we achieve the desired result,  $\delta p = A(q)\delta m$ , where  $A(q)$  is defined as

$$A(q) = J_p K(q)^{-1}J^T(JK(q)^{-1}J^T)^{-1}B_k. \quad (4)$$

### C. Control Law and Convergence

At each time step, we compute a desired displacement  $\delta p^d = p^d(t) - p + kI$ , where  $p^d(t)$  is a linear ramp from the initial point  $p$  toward the needle path (which helps reduce abrupt changes in force),  $I$  is an integral term, and  $k$  is an integral gain. We then compute the commanded manipulator displacement  $\delta m = gA(q)^{-1}\delta p^d$ , where  $g$  is a gain parameter. This controller provably converges to a fixed point if  $g$  and  $k$  are set low enough, under tissue modeling conditions on  $A(q)$  that are usually satisfied [11]. The values of  $g$  and  $k$  control the rate of convergence, and should be set as high as possible to ensure rapid convergence. We use a small amount of manual tuning to pick suitable parameters.

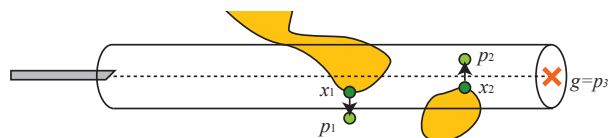


Fig. 2. Selecting points of interest  $p_1$  and  $p_2$  to displace sensitive tissues (shaded regions).

## V. PROCEDURE PLANNING

This section addresses automatic procedure planning for the phased manipulation controller. Especially under unilateral (pushing) manipulation, the needle path and manipulation points must be chosen carefully to ensure that contact is fixed during the duration of each phase. First, we describe a method to choose points of interest, assuming a given needle insertion path. Then, we describe a cost metric that measures how robustly a given manipulator location rejects disturbances. Finally, we describe a stochastic optimization that uses this cost metric to optimize all procedure parameters.

The  $n$  phases of the procedure correspond to  $n$  points of interest  $p_1, \dots, p_n$ . These points are sorted in the order in which the needle passes nearby. We set  $p_n$  to the target position  $g$ . The phases are chosen to drive each point to the needle path sequentially. Starting at  $k = 1$ , the controller drives  $p_k$  toward the needle path, and switches from  $p_k$  to  $p_{k+1}$  when the needle has passed  $p_k$ .

### A. Selecting Points of Interest

The following technique is given as input a needle path and an obstacle volume  $\mathcal{O}$ , which could be segmented from preoperative imaging, and automatically outputs points of interest that correspond to sensitive tissues that should be pushed away from the needle path. Examine the portion of  $\mathcal{O}$  inside a cylinder of width  $w$  around the needle path, and select the points  $x_1, \dots, x_{n-1}$  with maximum penetration distance. Then, for  $i = 1, \dots, n-1$ , shift the point  $x_i$  along its penetration direction by a distance  $\epsilon$  to obtain the  $i$ 'th point of interest  $p_i$  (Fig. 2). Thus, moving  $p_i$  onto the needle path will move  $x$  away from it. Choosing a suitable  $\epsilon$  is not difficult in practice. It should be set high enough to exceed measurement uncertainty, but not so high that excessive forces are applied by the manipulator.

### B. Selecting Manipulators and Force Profiles

The same manipulator could potentially be used for all phases of the procedure. If tissue does not tear at the needle tip, then once the needle passes the point of interest  $p_i$ , the manipulation forces can be removed while safely maintaining the position of  $p_i$ . If tissue tearing is a possibility, it may be safer to use a different manipulator for each phase.

Manipulation devices are primarily characterized by the types of forces they can apply. Simple *unilateral* manipulators use compressive (pushing) contact forces, and can, to some extent, shear the tissue using friction forces. Other types of manipulators may also apply tension forces, such as suction tubes, clamps, or adhesives. For a given device, we define a *force profile*, the set of forces that the manipulator

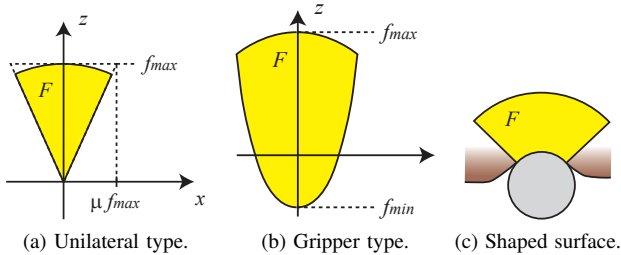


Fig. 3. Applicable forces for different manipulator types.

can apply on the tissue without breaking contact, slipping, or rolling. The force profile is a critical component of the planning procedure.

By convention, we represent a force profile  $F$  in a frame where the manipulator/tissue contact normal is oriented to the  $z$  axis. For a unilateral manipulator,  $F$  is approximately a cone (known as the *friction cone*), with apex at the origin, height equal to the actuator’s maximum force  $f_{max}$ , and base radius equal to  $f_{max}\mu$ , where  $\mu$  is the coefficient of friction between the manipulator and tissue (Fig. 3a). Manipulators that can apply tension forces have a force profile  $F$  that extends in the  $-z$  direction (Fig. 3b). The shape of  $F$  in the  $x$  and  $y$  directions will inevitably vary depending on the type of manipulator, and may not even be symmetric. In practice, we may be able to estimate  $F$  from patient-specific tactile sensing, or estimate a conservative inner approximation from mechanical models.

We remark that it may be beneficial to use unilateral manipulators with a large, rounded region of manipulator/tissue contact. This would reduce tissue strain and enable use of a set of contact normals rather than a single normal, which would increase the volume of  $F$  (Fig. 3c).

### C. Selecting Manipulation Points

Let  $p$  denote the point of interest that we wish to control with a manipulator  $M$ , and consider a potential manipulator placement  $m$ . The set of forces that  $M$  can apply without slipping or breaking contact is a set  $F'$  that is simply a reorientation of the force profile  $F$ . Following the linearized, quasistatic approximation of Sec. IV, we can compose this rotation with (3), to show that the set  $D$  of potential displacements of  $p$  is a linear transform of  $F$ . This set is used to evaluate a cost metric that measures the manipulator’s ability to reject disturbances (similar to [14]).

We approximate  $F$  as a convex polytope, such that the vertices of  $D$  are simply a linear transform of the vertices of  $F$ . We must ensure that the needle path  $r$  passes through  $D$  with a wide margin, because the margin approximates the size of disturbance that can be rejected. Disturbances along  $r$  can be corrected by insertion or retraction of the needle, so we only need to consider errors along a perpendicular plane. So, we project  $D$  and  $r$  onto the perpendicular plane, which produces a two-dimensional convex polygon  $D'$  and point  $v'$ , respectively. We then measure the *disturbance rejection margin*  $\alpha$  from  $v'$  to the edge of  $D'$  (Fig. 4b).

The cost metric also includes a term that measures the expected equilibrium force. We set  $\beta = \min_{x \in r \cap D} \|f(x -$

$p)\|$  where  $f(\delta p)$  measures the equilibrium force applied by the manipulator to displace  $p$  by  $\delta p$  (Fig. 4c). Since  $f(\delta p)$  is a linear function,  $\beta$  can be determined with some algebraic manipulation. The resulting cost metric is  $c(r, p, m) = 1/\alpha + w\beta$  for some positive weight  $w$ .

### D. Stochastic Optimization

We now wish to choose a needle insertion path  $r$  and a set of manipulator locations given a geometric model. We define the cost metric to be the sum of all single-phase cost metrics, as defined above. The set of insertion locations and directions are restricted to some set  $\mathcal{R}$ , and the set of manipulator locations are restricted to  $\mathcal{M}$ .

We use a stochastic method that creates a search tree by sampling parameters. The first branch chooses samples of the needle path  $r$ , drawn from  $\mathcal{R}$ . At this branch, we generate the points of interest  $p_1, \dots, p_n$  using the procedure in Sec. V-A. Here,  $n$  is a function of  $r$ , and determines the height of the subtree. In each subtree, each subsequent branch samples from  $\mathcal{M}$  to assign a location  $m_i$  to manipulator  $i$ . Such a branch has cost  $c(r, p_i, m_i)$ . The optimization tries to find a minimum cost path that assigns all parameters.

To accelerate the search, we maintain a current minimum cost estimate  $C_{min}$ , which can be used to prune out infeasible and high-cost branches. We also use a best-first strategy, where needle paths are prioritized by distance to the target, and manipulator locations are prioritized by lowest cost. Once we have found a fairly low-cost procedure, local perturbations may improve the solution further.

Implementing this procedure, we find that for unilateral manipulators, it is preferable to shift the needle insertion point along the contact normal. The manipulator will then apply an initial load to align the needle shaft and the target. This allows correction of targeting errors in the  $-z$  direction by reducing the load, and correction of tangential errors by applying frictional shear forces.

## VI. EXPERIMENTS IN SIMULATION

### A. Obstacle Avoidance

We simulate a two-dimensional, quasistatic mass-spring model of the tissue. Nodes are arranged in a  $7 \times 20$  grid, with 1cm spacing. Each link is modeled as a linearly elastic truss with a  $0.25\text{cm} \times 0.25\text{cm}$  cross section and elastic modulus of 60kPa (this approximates the stiffness of soft tissue). The corners and rightmost nodes are fixed. The needle is inserted from left to right. The points at which the needle pierces links are constrained to move only in the  $x$  direction, and under viscous friction. This simulation is indeed highly simplified, but captures the essential components of a manipulation system. We would expect to see more accurate estimates of the applied force and tissue strain with better models of tissue (for example, 3D finite element simulation, with biologically accurate constitutive models [4]) and tissue-needle interaction (for example, with more accurate needle cutting forces [10], friction forces, and element remeshing).

The manipulation controller does not have access to the simulator’s model, and uses an entirely different model to

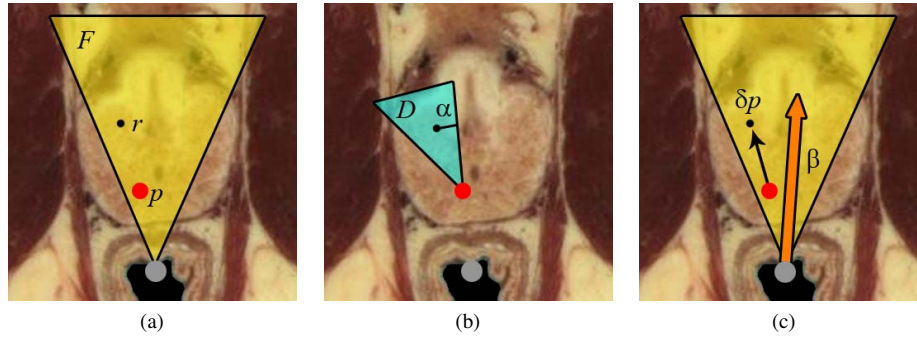


Fig. 4. Illustrating the quality metric in a slice of the prostate, viewed down the needle path  $r$ . The manipulator is depicted as a gray circle. (a) The force profile  $F$  and a point of interest  $p$ . (b) Potential displacements  $D$  of the point of interest, and the disturbance rejection margin  $\alpha$ . (c) The approximate equilibrium force, with magnitude  $\beta$ .

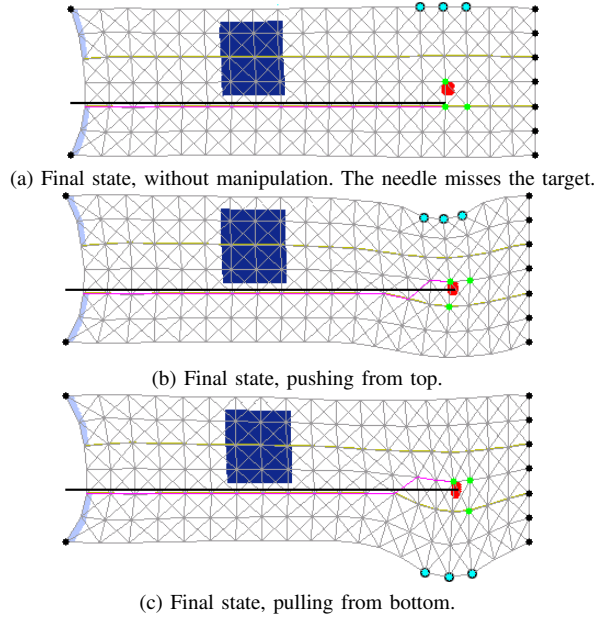


Fig. 5. Improving accuracy using target manipulation. Large black circles indicate fixed nodes. Manipulated nodes are highlighted in blue.

compute the feedforward manipulator displacement. In fact, it uses the simplest possible model: a linear spring. Our experiments show that even with such a crude approximation, the controller works quite well.

Fig. 5 shows an example where the target is misaligned by 5.9mm from the needle insertion path. This misalignment could have been deliberately chosen to avoid an obstacle (the shaded rectangle), or have occurred by accident. Without manipulation, the target is missed by approximately 5.9mm. Applying compression from the top reduces targeting error to 0.54mm, with a maximum downward force of 1.11N. Applying tension from the bottom reduces targeting error to 1.46mm with a maximum force of 1.56N.

### B. Obstacle Avoidance

We performed several experiments to test how manipulation can help guide the needle around sensitive tissues. Fig. 6 depicts the setup: two obstacles, 1.25cm apart, obstruct the passage to a distant target 15cm away. The system manipulates the obstacle in the first phase, and manipulates the target in the second. The point of interest for the first phase is located in the center of the passage. Table I reports

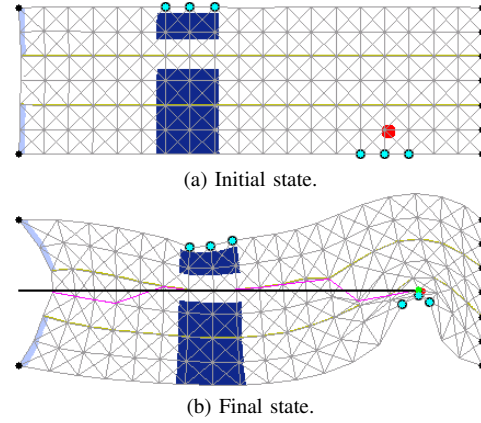


Fig. 6. Improving accessibility and accuracy by pushing the obstacle from above and the target from below.

the results for various vertical displacements of the target position, and horizontal and vertical displacements of the obstacles. The system is able to reduce the targeting error to about 1mm in all cases, and the needle passes through the obstacles with a wide margin. As might be expected, the size of target and obstacle displacements are highly correlated with larger manipulation forces and larger tissue strain.

### C. Application to Prostate Brachytherapy

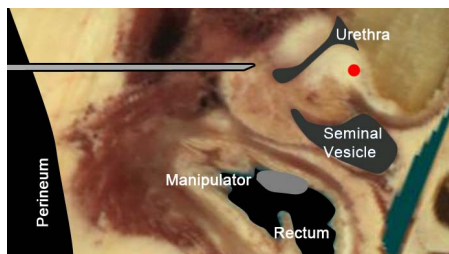
We apply our system to a simulation of a needle insertion for prostate brachytherapy, and use manipulation for both obstacle avoidance and accuracy improvement (Fig. 7). In the simulation plane, the urethra and seminal vesicles form obstacles, with a gap of approximately 0.7cm. We simulate an 11 x 18 mass-spring grid, where each cell is approximately 0.7cm x 0.7cm. Boundary nodes are fixed. Both the obstacle and targeting phases use the same manipulator in the rectum. The manipulator is constrained to move along a  $103^\circ$  heading. Running our simulation, the needle successfully passes between the obstacles, with 2.1mm clearance, and reaches the target, with 1.49mm error. The maximum force applied at the manipulator was 8.06N.

## VII. CONCLUSION

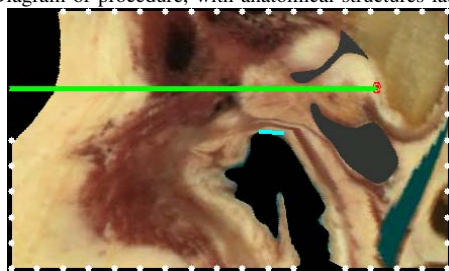
We have proposed the use of single-point tissue manipulation using a robotic device to improve the accuracy and accessibility of medical needle insertion procedures. We present a closed-loop controller that guides a needle toward

TABLE I  
STATISTICS FOR SIMULTANEOUS OBSTACLE AND TARGET MANIPULATION.

Target $y$ position, relative to needle (mm)	Obstacle gap position, relative to needle (mm)	Final targeting error (mm)	Closest distance to obstacle (mm)	Maximum applied force (N)	Maximum strain
0	(54,0)	1.05	4.17	0.133	0.03
-14.5	(54,-4)	0.94	4.62	13.96	0.19
-21.8	(50,3.74)	0.50	5.84	8.49	0.75
-21.8	(70,9.52)	0.72	6.22	16.84	0.78
-21.8	(110,10.75)	0.87	4.47	6.76	0.93
-18.8	(110,13.76)	0.87	3.85	14.978	0.85
21.8	(75,-10.25)	0.75	4.86	4.36	0.53



(a) Diagram of procedure, with anatomical structures labeled.



(b) Final configuration of simulated procedure.

Fig. 7. Simulation of a prostate needle insertion. Image is an oblique slice from The Virtual Human Project dataset.

a target while avoiding sensitive tissues, and an automatic procedure planning technique that selects a needle insertion path and manipulation points. In 2D deformable tissue simulations, including an application to prostate brachytherapy, we showed the method can reduce targeting errors from over 2cm to less than 1mm. It can also push sensitive tissues by over 1cm to avoid needle puncture.

An immediate goal for future work is to evaluate our technique with more sophisticated 3D tissue models and needle-tissue interaction models. More accurate tissue injury models, such as those that include duration of applied load [5], could be incorporated in procedure planning. We would also like to test the automated procedure planner with various medical applications, including multiple-seed prostate brachytherapy treatments. A long-term goal is to move from simulations to clinical settings. We would like to target specific clinical applications (especially prostate brachytherapy) and experiment with real hardware. Other future work could address slip-avoiding controllers that use tactile sensing, new manipulation models (such as multi-point manipulation or passive fixturing), or tissue manipulation combined with steerable needles.

## VIII. ACKNOWLEDGEMENT

We thank the following colleagues for their insights and contributions: G. Fichtinger of Queens University, A. Oka-

mura, N. Cowan, G. Chirikjian, R. Taylor, V. Kallem, and K. Reed of Johns Hopkins University, and A. Cunha, I.-C. Hsu, and J. Pouliot of UCSF.

## REFERENCES

- [1] R. Alterovitz and K. Goldberg. *Motion Planning in Medicine: Optimization and Simulation Algorithms for Image-Guided Procedures*. Springer-Verlag, Berlin Heidelberg, 2008.
- [2] R. Alterovitz, K. Goldberg, J. Pouliot, I.-C. Hsu, Y. Kim, S. Noworolski, and J. Kurhanewicz. Registration of MR prostate images with biomechanical modeling and nonlinear parameter estimation. *Med. Phys.*, 33(2):446–454, 2006.
- [3] R. Alterovitz, J. Pouliot, R. Tashereau, I.-C. Hsu, and K. Goldberg. Sensorless planning for medical needle insertion procedures. In *Proc. IEEE/RSJ Int. Conf. on Intelligent Robots and Systems (IROS)*, volume 3, pages 3337–3343, 2003.
- [4] J. R. Crouch, C. M. Schneider, J. Wainer, and A. M. Okamura. A velocity-dependent model for needle insertion in soft tissue. *Proc. 8th Int. Conf. on Medical Image Computing and Computer Assisted Intervention*, 3750:624632, 2005.
- [5] S. De, J. Rosen, A. Dagan, B. Hannaford, P. Swanson, and M. Sinanan. Assessment of tissue damage due to mechanical stresses. *Int. J. of Robotics Research*, 26(11-12):1159–1171, 2007.
- [6] E. Dehghan and S. E. Salcudean. Needle insertion point and orientation optimization in non-linear tissue with application to brachytherapy. In *Proc. IEEE Int. Conf. Robotics and Automation*, page 22672272, 2007.
- [7] S. DiMaio and S. Salcudean. Needle steering and motion planning in soft tissues. *IEEE Trans. Biomedical Engineering*, 52(6):965–974, 2005.
- [8] M. Eloubeidi, D. Jhala, D. Chieng, V. Chen, I. Eltoun, S. Vickers, C. M. Wilcox, and N. Jhala. Yield of endoscopic ultrasound-guided fine-needle aspiration biopsy in patients with suspected pancreatic carcinoma. *Cancer*, 99(5):285–292, October 2003.
- [9] D. Glozman and M. Shoham. Image-guided robotic flexible needle steering. *IEEE Trans. Robotics*, 23(3):459–467, 2007.
- [10] M. Heverly, P. Dupont, and J. Triedman. Trajectory optimization for dynamic needle insertion. In *Proc. IEEE Intl. Conf. on Robotics and Automation*, 2005.
- [11] S. Hirai and T. Wada. Indirect simultaneous positioning of deformable objects with multi-pinching fingers based on an uncertain model. *Robotica*, 18:3–11, 2000.
- [12] S. Khattar, S. Torp-Pedersen, T. Horn, I. Krogh-Pedersen, M. Court-Payen, and T. Lorentzen. Ultrasound-guided biopsy of palpable breast masses. *European Journal of Ultrasound*, 6(1):1–7, August 1997.
- [13] V. Mallapragada, N. Sarkar, and T. Podder. Robot assisted real-time tumor manipulation for breast biopsy. In *Proc. IEEE Intl. Conf. on Robotics and Automation*, 2008.
- [14] B. Mishra. Grasp metrics: Optimality and complexity. In K. Goldberg, D. Halperin, J. Latombe, and R. Wilson, editors, *Algorithmic Foundations of Robotics*, pages 137–166. A.K. Peters, 1995.
- [15] K. B. Reed, V. Kallem, R. Alterovitz, K. Goldberg, A. M. Okamura, and N. J. Cowan. Integrated planning and image-guided control for planar needle steering. In *Proc. IEEE/RAS-EMBS Intl. Conf. on Biomedical Robotics and Biomechanics*, pages 819–824, 2008.
- [16] R. Taschereau, J. Pouliot, J. Row, and D. Tremblay. Seed misplacement and stabilizing needles in transperineal permanent prostate implants. *Radiotherapy and Oncology*, 55(1):59–63, 2000.
- [17] R. J. Webster III, J. S. Kim, N. J. Cowan, G. S. Chirikjian, and A. M. Okamura. Nonholonomic modeling of needle steering. *Int. J. of Robotics Research*, 25(5-6):509–525, 2006.